Chinese Journal of Natural Medicines

Sesquiterpenoids from *Tussilago farfara*: full structure elucidation, anti-diabetic and anti-inflammatory signaling pathways

Hao Zheng, Yang Li, Yujia Zhang, Zhixuan Li, Dongli Li, Jucai Xu, Jianjun Zhang, Ligen Lin, Lishe Gan

Citation: Hao Zheng, Yang Li, Yujia Zhang, Zhixuan Li, Dongli Li, Jucai Xu, Jianjun Zhang, Ligen Lin, Lishe Gan, Sesquiterpenoids from *Tussilago farfara*: full structure elucidation, anti-diabetic and anti-inflammatory signaling pathways, Chinese Journal of Natural Medicines, 2026, 24(3), 373-384. doi: 10.1016/S1875-5364(26)61111-9.

View online: https://doi.org/10.1016/S1875-5364(26)61111-9

Chinese Journal of Natural Medicines 24 (2026) 373-384

Contents lists available at ScienceDirect

Chinese Journal of Natural Medicines

journal homepage: www.cjnmcpu.com/

Original article

Sesquiterpenoids from *Tussilago farfara*: full structure elucidation, anti-diabetic and anti-inflammatory signaling pathways

Hao Zheng[a,b,c,Δ], Yang Li[b,d,Δ], Yujia Zhang[b,Δ], Zhixuan Li[b], Dongli Li[b], Jucai Xu[b], Jianjun Zhang[e], Ligen Lin[c,*], Lishe Gan[a,b,*]

[a] *School of Pharmaceutical Sciences, The First Affiliated Hospital of Zhejiang Chinese Medical University, Hangzhou 311402, China*
[b] *School of Pharmacy and Food Engineering, International Healthcare Innovation Institute, Wuyi University, Jiangmen 529020, China*
[c] *State Key Laboratory of Quality Research in Chinese Medicine, Institute of Chinese Medical Sciences, University of Macau, Macau 999078, China*
[d] *Nanchong Vocational College of Science and Technology, Nanchong 637000, China*
[e] *The First Affiliated Hospital of Zhejiang Chinese Medical University (Zhejiang Provincial Hospital of Traditional Chinese Medicine), Hangzhou 310003, China*

ARTICLE INFO

Article history:
Received 21 February 2025
Revised 6 May 2025
Accepted 13 May 2025
Available online 20 March 2026

Keywords:
Sesquiterpenoids
Quantum chemical calculations
2,3-seco Oplopane
Tussilago farfara
Anti-diabetes
Anti-inflammation

ABSTRACT

Four new sesquiterpenoids (**1**–**4**), including the first reported instance of a novel 2,3-seco oplopane carbon skeleton (**1**), together with 19 known analogues, were isolated from the flower buds of *Tussilago farfara* (coltsfoot). The challenging determination of relative and absolute configurations—particularly in flexible side chains and substituents—was achieved for the first time through an integrated approach combining spectroscopic analyses, chemical derivatization, chiral gas chromatography (GC), and quantum chemical calculations. All compounds were evaluated for anti-diabetic activity using an insulin-stimulated glucose uptake model in C2C12 myotubes and for anti-inflammatory activity *via* a lipopolysaccharide (LPS)-induced nitric oxide (NO) inhibition assay in RAW264.7 macrophages. Six compounds significantly enhanced glucose uptake, and mechanistic investigation of compound **3** revealed activation of the insulin receptor substrate 1 (IRS-1)/protein kinase B (Akt)/glycogen synthase kinase 3β (GSK-3β) signaling pathway. Twenty-one compounds exhibited marked inhibition of NO production; among them, compounds **2** and **6** dose-dependently suppressed inducible nitric oxide synthase (iNOS) expression and nuclear factor κB (NF-κB) phosphorylation.

1. Introduction

Tussilago farfara L. (Asteraceae), commonly known as coltsfoot, is a perennial herb native to West Europe, North Africa, and parts of Asia, including China, India, Iran, and Pakistan [1]. It was historically considered a common weed in winter wheat and corn fields, as well as along roadsides and stream banks. However, coltsfoot has since been recognized for its potent therapeutic effects on cough and asthma. Today, it is marketed as an herbal supplement due to its anti-tussive, anti-microbial, and anti-inflammatory properties [2]. In traditional Chinese medicine (TCM), the flower buds of *T. farfara* (known as Kuandonghua) are widely used in clinical practice for treating respiratory conditions such as cough and asthma [3].

Phytochemical studies have identified sesquiterpenoids as the primary constituents of coltsfoot, although the relative and absolute configurations of the flexible side chain and substituents in many structures remain unresolved [2, 4–5]. Other components, including triterpenoids, alkaloids, flavonoids, and phenolic compounds, are present in smaller quantities [6], among which pyrrolizidine alkaloids are notable for their hepatotoxicity [7]. In contrast, sesquiterpenoids—primarily of the oplopane and bisabolene types—have demonstrated a range of pharmacological activities, including anti-inflammatory [2–3], anti-asthmatic [3], anti-hepatic steatosis [8], anti-oxidant [8], anti-osteoporotic [9], anti-tumor [10], anti-platelet [11], and neuroprotective effects [12]. Consequently, sesquiterpenoids are regarded as one of the most important groups of bioactive constituents in *T. farfara*.

As part of our ongoing research on terpenoids with anti-diabetic potential [13–15], the sesquiterpenoids in *T. farfara* were selected for further phytochemical and pharmacological investigation, given their demonstrated efficacy in ameliorating glucose metabolic disorders and enhancing energy metabolism in high-fat diet-induced non-alcoholic fatty liver disease (NAFLD) mice [8]. Insulin resistance represents the central pathological feature of type 2 diabetes mellitus (T2DM) [16]. Skeletal muscle, as a primary target tissue of insulin, accounts for more than 80% of peripheral glucose uptake [17]. Impairment of skeletal muscle function is therefore considered a key initiating factor in the development of T2DM [18]. Clinically, insulin sensitizers such as metformin and rosiglitazone are the most widely prescribed anti-diabetic agents [19–20]. However, their long-term use is associated with adverse effects, including diarrhea, nausea, and the emergence of drug resistance, underscoring the need to discover novel, safe, and effective insulin-sensitizing agents [21].

In this study, 23 sesquiterpenoids were isolated from the flower buds of *T. farfara* using phytochemical techniques. Their

* Corresponding author.
E-mail addresses: ligenl@umac.mo (L. Lin); lsgan@zcmu.edu.cn (L. Gan)
Δ These authors contributed equally to this work.

https://doi.org/10.1016/S1875-5364(26)61111-9

structures and configurations—particularly those of the flexible side chain and substituents—were determined through a combination of spectroscopic methods, chemical derivatization, chiral chromatography, and quantum chemical calculations. Notably, a sesquiterpene (**1**) featuring a novel 2,3-seco oplopane carbon skeleton and three additional new sesquiterpenes (**2**–**4**) were identified. These compounds were evaluated for anti-diabetic activity using a glucose uptake assay in C2C12 myotubes and for anti-inflammatory activity *via* a nitric oxide (NO) inhibition assay in lipopolysaccharide (LPS)-induced RAW264.7 macrophages. Furthermore, the underlying signaling pathways of the most active compounds were investigated using Western blot analysis.

2. Result and discussion

Tussilagofarone (**1**) was isolated as a colorless oil. high-resolution electrospray ionization mass spectrometry (HR-ESI-MS) revealed a pseudo-molecular ion peak at *m/z* 501.2825 $[M + Na]^+$ (Calcd. for $C_{27}H_{42}NaO_7$, 501.2823), indicating 7 degrees of unsaturation. The IR spectrum showed absorption bands characteristic of carbonyl and double bond functionalities at 1744, 1711, and 1648 cm^{-1}. The ^1H nuclear magnetic resonance (NMR) spectrum (Table 1) displayed signals corresponding to seven methyl groups: δ_H 0.85 (6H, H_3-12 and H_3-13, d, J = 6.7 Hz), 0.97 (6H, H_3-15 and H_3-4′, t, J = 7.5 Hz), 1.09 (H_3-5″, t, J = 7.3 Hz), 1.21 (H_3-5′, d, J = 7.0 Hz), and 2.16 (H_3-6″, s). Additionally, a methoxy group was observed at δ_H 3.69 (s), along with signals for a terminal double bond methylene at δ_H 5.19 (1H, d, J = 1.8 Hz) and 4.69 (1H, d, J = 1.8 Hz). In the ^{13}C NMR spectrum (Table 1), resonances were assigned to a ketone carbonyl at δ_C 215.2 (C-3), three ester carbonyls at δ_C 175.6 (C-1′), 166.2 (C-1″), and 169.9 (C-2), and two double bonds at δ_C 166.2, 114.9, 144.9, and 112.5. The methoxy group was further confirmed by a carbon signal at δ_C 52.7. These spectroscopic data suggested a sesquiterpenoid bearing two short-chain acid esters, structurally similar to known sesquiterpenoids from *T. farfara* [2]. Besides the methoxy group, the presence of methyl-senecioyloxy and methylbutyryloxy moieties was inferred by comparison with literature data [22]. The remaining fifteen-carbon framework indicated a sesquiterpenoid featuring one terminal double bond, one ketone carbonyl, one ester carbonyl, and one terminal methyl group (Fig. 1). These structural characteristics differ significantly from those of oplopane and

Table 1 ^1H (500 MHz) and ^{13}C NMR (125 MHz) data for compounds **1**–**4** in $CDCl_3$ (J in Hz).

No.	1		2		3		4	
	δ_H	δ_C	δ_H	δ_C	δ_H	δ_C	δ_H	δ_C
1	5.38 (1H, d, 1.5)	70.4	5.37 (1H, d, 4.0)	72.9	5.94 (1H, d, 12.2)	75.5	–	183.3
2	–	169.9	–	210.0	–	202.4	–	143.9
3	–	215.2	2.17 (1H, br d, 10.3)	59.8	–	78.5	–	143.4
4	2.85 (1H, dd, 10.8, 11)	53.6	2.37 (1H, m)	43.4	4.23 (1H, t, 3.6)	64.7	4.28 (1H, br s)	68.6
5	2.13 (1H, m)	41.8	1.85 (1H, m)	44.3	β 2.29 (1H, dt, 15.0, 3.6) α 2.70 (1H, ddd, 15.0, 12.2, 3.6)	35.4	β 3.28 (1H, dd, 14.9, 3.4) α 2.84 (1H, m)	35.3
6	β 1.95 (1H, m) α 1.38 (1H, m)	29.8	β 2.00 (1H, m) α 1.46 (1H, m	30.5	3.06 (1H, td, 12.2, 3.6)	40.1	–	127.8
7	5.51 (1H, dd, 1.4, 3.4)	73.7	5.55 (1H, dd, 3.1, 3.0)	73.8	–	147.3	–	145.6
8	–	144.9		141.0	5.19 (1H, dd, 6.0, 8.0)	75.4	5.51 (1H, t, 7.4)	74.3
9	3.45 (1H, dd, 10.8, 1.5)	42.4	2.55 (1H, dd, 12.2, 4.0)	46.6	2.40 (2H, m)	32.2	2.54 (1H, ddd, 14.7, 7.4, 7.4) 2.33 (1H, dt, 14.7, 7.4, 7.4)	31.3
10	a 5.19 (1H, d, 1.8) b 4.69 (1H, d, 1.8)	112.5	5.18 (1H, br s) 4.80 (1H, br s)	113.4	5.09 (1H, t, 6.3)	119.4	5.03 (1H, br t, 7.4)	118.1
11	1.50 (1H, m)	27.9	1.95 (1H, m)	28.3	–	134.5	–	135.8
12	0.85 (3H, d, 6.7)	21.6	0.96 (3H, d, 6.8)	21.6	1.67 (3H, br s)	25.6	1.68 (3H, s)	25.9
13	0.85 (3H, d, 6.7)	15.8	0.89 (3H, d, 6.8)	15.6	1.62 (3H, br s)	18.9	1.63 (3H, s)	18.1
14	a 2.80 (1H, m) b 2.42 (1H, m)	39.4	4.06 (1H, qd, 6.6, 1.5)	68.1	a 5.28 (1H, br s) b 5.17 (1H, br s)	112.6	1.95 (3H, s)	13.8
15	0.97 (3H, t, 7.5)	6.6	1.47 (3H, d, 6.6)	22.8	1.50 (3H, s)	21.7	1.96 (3H, s)	15.3
1′	–	175.6	–	176.0	–	166.6	–	171.1
2′	2.52 (1H, m)	41.1	2.39 (1H, m)	41.4	5.68 (1H, q, 1.4)	113.5	2.55 (1H, m) 2.33 (1H, m)	40.9
3′	1.77 (1H, m) 1.53(1H, m)	26.8	1.67 (1H, m) 1.44 (1H, m)	26.7	–	164.0	1.98 (1H, br d,7.3)	32.0
4′	0.97 (3H, t, 7.5)	11.6	0.87 (3H, t, 7.4)	11.6	2.16 (2H, qd, 7.5, 1.4)	34.0	1.30 (1H, m) 1.45 (1H, m)	29.5
5′	1.21 (3H, d, 7.0)	16.7	1.13 (3H, d, 5.5)	16.5	1.05 (3H, t, 7.5)	11.9	0.92 (3H, t, 5.0)	11.4
6′	/	/	/	/	2.12 (3H, d 1.3)	19.1	1.04 (3H, d, 5.0)	19.8
1″	–	166.2	–	165.9	–	167.7	–	168.2
2″	5.73 (1H, s)	114.9	5.61 (1H, q, 1.2)	114.6	–	128.1	–	127.2
3″	–	162.3	–	162.7	6.08 (1H, qq, 7.2, 1.5)	139.1	6.14 (1H, qq, 7.3, 1.5)	140.4
4″	2.18 (1H, m) 2.33 (1H, m)	34.0	2.16 (2H, m)	33.9	1.98 (3H, d, 7.2)	15.9	1.98 (3H, br d, 7.3)	16.1
5″	1.09 (3H, t, 7.3)	12.1	1.06 (3H, t, 7.4)	12.0	1.90 (3H, d, 1.5)	20.8	1.88 (3H, d, 1.6)	20.7
6″	2.16 (3H, s)	19.1	2.15 (3H, d, 1.2)	19.0	/	/	/	/
OCH_3 /OH	3.69 (3H, s)	52.7	/	/	5.09 (1H, m)	/	/	/

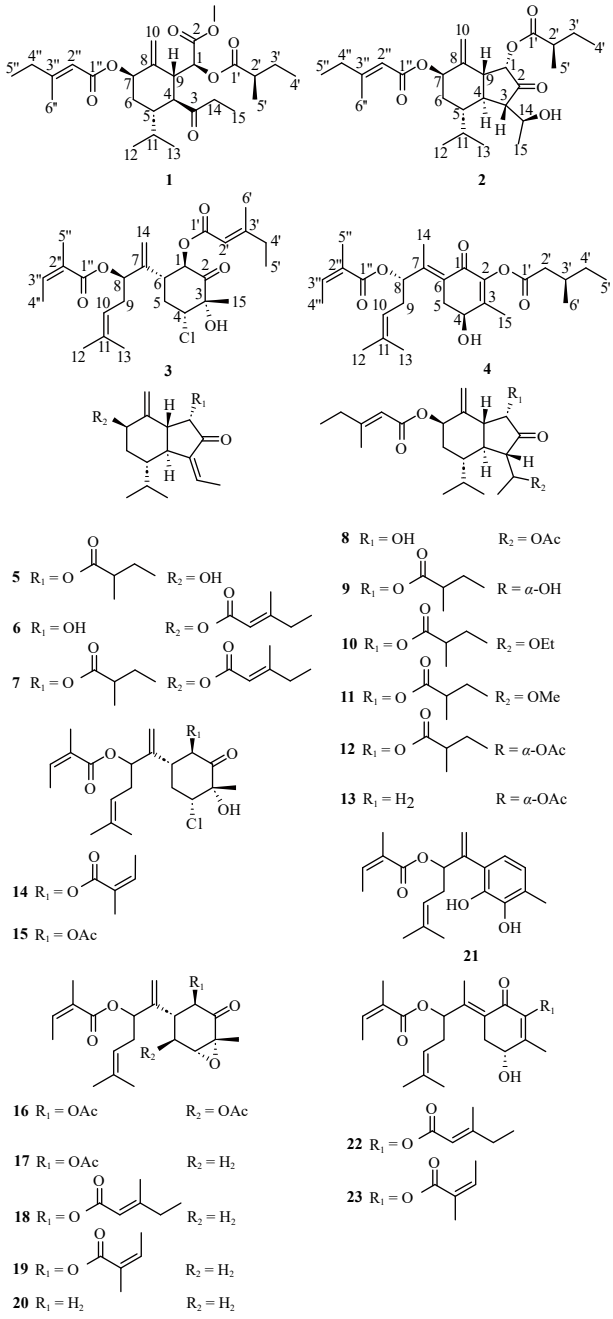

Fig. 1 Chemical structures of **1**–**23**.

bisabolane-type sesquiterpenoids, suggesting a novel carbon skeleton for compound **1**. Further 2D NMR experiments enabled the elucidation of the planar structure. A heteronuclear single quantum correlation (HSQC) experiment facilitated the assignment of all protonated carbons. In the ^{1}H–^{1}H correlation spectroscopy (COSY) spectrum, correlations were observed for H-1/H-9, H-9/H-4, H-4/H-5, H-5/H-6, H-6/H-7, and H-5/H-11, H-11/H_3-12, and H-11/H_3-13, establishing a nine-carbon spin system (Fig. 2). The terminal double bond was positioned between CH-9 and CH-7, forming a six-membered ring, as supported by heteronuclear multiple bond correlations (HMBCs) from H2-10 to C-7 and C-9. HMBCs from H-9 and the methoxy group protons to the ester carbonyl C-2 indicated a 2,3-seco oplopane sesquiterpenoid skeleton. Additional HMBCs from H-5 and H_3-15 to the ketone carbonyl at C-3 confirmed the unprecedented carbon framework. The methyl-senecioyloxy and methylbutyryloxy groups are commonly found in sesquiterpenoids from *T. farfara*; their identities were verified by comparison with reported analogues [22] and confirmed by key HMBCs shown in Fig. 2. Their attachment to C-7 and C-1 *via* ester linkages was established by HMBCs of H-7/C-1″ and H-1/C-1′, respectively. Thus, the planar structure of compound **1** was fully determined. Compared to the typical oplopane-type sesquiterpene scaffold prevalent in Asteraceae plants, compound **1** features a novel 2,3-seco oplopane carbon skeleton.

The configuration of compound **1** was determined using a combination of chemical, spectroscopic, and computational approaches. First, the absolute configuration at C-2′ of the methylbutyryloxy substituent was established by base hydrolysis followed by methylation and chiral gas chromatography (GC) analysis, comparing the derivatives with authentic standards (see Supplementary data S33). Comparison of the methylation products derived from (*S*)- and (*R*)-2-methylbutyric acids allowed assignment of the *R* configuration at C-2′. Nuclear Overhauser effect spectroscopy (NOESY) correlations between H-9/H-5, H-9/H2-14, and H-5/H-6β indicated their co-facial orientation, which was arbitrarily assigned as *β*. Conversely, *α*-orientation of H-4, H-1, H_2-10, and H-6α was confirmed by corresponding NOESY correlations depicted in Fig. 3. This assignment was further supported by relatively large coupling constants of $J_{4,9}$ = 10.8 Hz and $J_{4,5}$ = 11.0 Hz, consistent with axial orientations on a six-membered ring. The small coupling constants between H-7 (dd, J = 3.4, 1.4 Hz) and H_2-6 indicated an equatorial position for H-7. NOESY correlations of H-2″ with H_2-4" and H-5" demonstrated an *E* configuration for the double bond in the side chain. The configuration at C-1 remained ambiguous due to free rotation around the C-9–C-1 bond, prompting quantum chemical calculation of

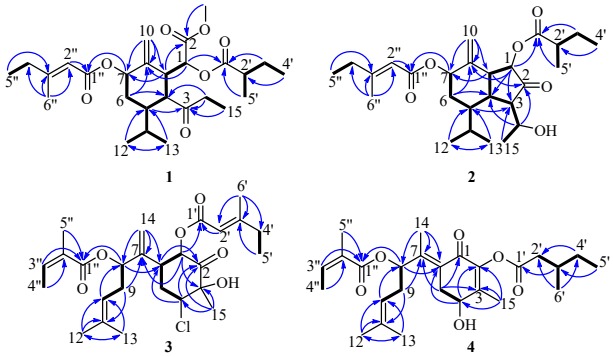

Fig. 2 ^{1}H–^{1}H COSY and Key HMBC correlations of **1**–**4**.

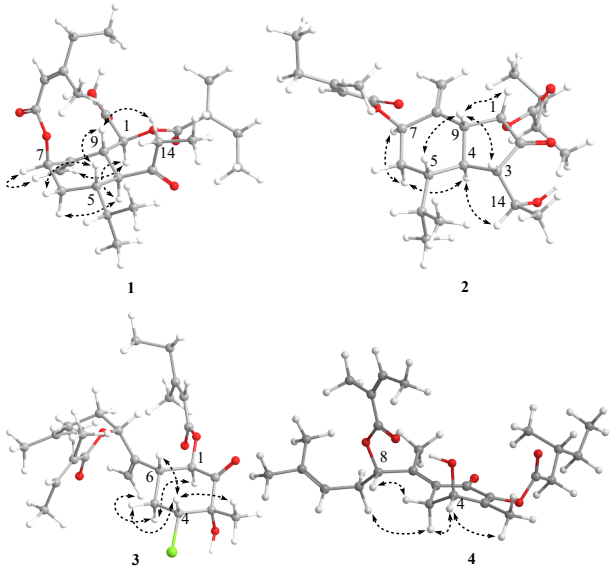

Fig. 3 Key NOESY correlations of **1**–**4**.

NMR chemical shifts for the two possible diastereomers. Conformational analysis and geometry optimization were performed at the density functional theory (DFT) level, followed by gauge-independent atomic orbital (GIAO) calculations of ^{1}H and ^{13}C NMR chemical shifts for 1S^*- and 1R^*-**1** at the mPW1PW91/6-31 + g (d,p) level. The experimental and calculated data were evaluated using the improved DP4 + probability method for isomeric compounds. The final score of 1S^*-**1** (100.00%) showed an absolute advantage over 1R^*-**1** (0%), supporting the relative configuration as 1S^*,4S^*,5S^*,7R^*,9R^*,2'R-**1** (Fig. 4). Linear correlation and differential analysis of ^{13}CNMR chemical shifts for the two possible isomers yielded consistent results. Finally, the absolute configuration was confirmed by electronic circular dichroism (ECD) calculations compared with the experimental spectrum. As shown in Fig. 5, theoretical ECD spectra for 1*R*,4*R*,5*R*,7*S*,9*S*,2'*R*-**1** and 1*S*,4*S*,5*S*,7*R*,9*R*,2'*R*-**1** were computed and compared with the experimental curve. Both the experimental ECD spectrum of **1** and the theoretical spectrum for 1*S*,4*S*,5*S*,7*R*,9*R*,2'*R*-**1** exhibited a sequence of positive, negative, and positive Cotton effects, whereas the curve for 1*R*,4*R*,5*R*,7*S*,9*S*,2'*R*-**1** was opposite. Therefore, the absolute configuration of tussilagofarone (**1**) was assigned as 1*S*,4*S*,5*S*,7*R*,9*R*,2'*R*.

The molecular formula of **2** was determined as $C_{26}H_{40}O_6$ by HR-ESI-MS, which showed a pseudo-molecular ion peak at *m/z* 471.2709 $[M + Na]^+$ (calcd for $C_{26}H_{40}O_6Na$, 471.2717). Relative to compound **1**, the ^{1}H NMR spectrum of **2** (Table 1) exhibited similar signals for a terminal double bond methylene at δ_H 5.18 and 4.80 (both br s, H_2-10), and three oxygen-bearing methines at δ_H 5.37 (1H, d, J = 4.0 Hz, H-1), 5.55 (1H, dd, J = 3.1, 3.0 Hz, H-7), and 4.06 (1H, qd, J = 6.6, 1.5 Hz, H-14). A methyl group attached to a double bond appeared at δ_H 2.15 (3H, br s, H_3-6″) and an olefinic methine at δ_H 5.61 (1H, q, J = 1.2 Hz, H_3-2″, confirming the methyl-senecioyloxy moiety. Two mutually coupled methyl groups at δ_H 0.96 (3H, d, J = 6.8 Hz) and 0.89 (3H, d, J = 6.8 Hz) indicated an isopropyl group. In the ^{13}C NMR spectrum, the methyl-senecioyloxy moiety was confirmed by characteristic signals at δ_C 165.9 (C-1″), 162.7 (C-3″), 114.6 (C-2″), 33.9 (C-4″), 19.0 (C-6″), and 12.0 (C-5″), comparable to those in **1**. Signals for the terminal double bond at δ_C 141.0 (C-8) and 113.4 (C-10), the ketone carbonyl at δ_C 210.0 (C-2), another ester carbonyl at δ_C 176.0 (C-1′), and three oxygen-bearing carbons at δ_C 73.8 (C-7), 72.9 (C-1), and 68.1 (C-14) were all observed. Collectively, these data indicated that **2** is a typical oplopane-type sesquiterpenoid, closely related to 7β-[3'-ethylcrotonoyloxy]-14-hydroxy-lα-[2'-methylbutyryloxy]-notonipetranone (**9**) [22-23]. Although the NMR data of **9** have not been fully assigned, comparison of 1D NMR spectra revealed differences: the coupling constant $J_{14,3}$ changed from 4.5 in **9** to 1.5 in **2**, the chemical shift of H_3-15 shifted from δ_H 1.20 in **9** to δ_H 1.47 in **2**, and the carbonyl carbon resonance moved from δ_C 214.5 in **9** to δ_C 210.0 in **2**. These changes suggest that **2** may be the 14-epimer of **9**. The HSQC, ^{1}H–^{1}H COSY, and HMBC spectra confirmed the oplopane [6,5]-bicyclic skeleton of **2** (Fig. 2). Key HMBCs from H-7 to C-1″ and from H-1 to C-1′ confirmed the positions of the ester substituents. Relative configurations at C-1, C-3, C-4, C-5, C-7, and C-9 were verified by NOESY correlations: H-1/H-9, H-9/H-3, H-9/H-5 indicated β-oriented protons, while H-4/H-6α and H-6α/H-7 indicated α-oriented protons. The stereochemistry at H-9, H-1, H-4, and H-3 was further inferred from coupling constants: $J_{1,9}$ = 4.0 Hz (*cis*), $J_{9,4}$ = 12.2 Hz (*trans*), and $J_{4,3}$ = 10.3 Hz (*trans*). NOESY correlations of H-2″/H-4″ and H-2″/H-5″ (Fig. 3) indicated an *E* configuration for the side chain double bond. As in **1**, the absolute configuration at C-2′ of the methylbutyryloxy group was determined to be *R*. Based on comparison with **9** and quantum chemical calculations of NMR chemical shifts for 14S^*-**2** and 14R^*-**2** using the GIAO method at the mPW1PW91/6-311G (d,p) level, followed by DP4 + probability analysis and linear correlation and differential analyses of ^{13}C NMR shifts (Fig. 6), the relative configuration was assigned. The 14S^*-**2** isomer showed a higher linear correlation coefficient (R^2 = 0.9972) and a DP4 + probability score of 77.93%, compared to 14R^*-**2**. ECD calculations further confirmed the absolute configuration as 1*S*,3*S*,4*S*,5*S*,7*R*,9*R*,14*S*,2'*R*-**2**, based on a matching ECD curve showing first negative and second positive Cotton effects (Fig. 5). Hence, the structure of **2** was assigned as 7β-[3'-ethylcrotonoyloxy]-14epi-hydroxy-lα-[2'-methylbutyryloxy]-notonipetranone

Tussfararin G (**3**) was isolated as a colorless oil. HR-ESI-MS displayed a pseudo-molecular ion peak at *m/z* 503.2167 $[M + Na]^+$, corresponding to a molecular formula of $C_{26}H_{37}ClO_6$ (calcd. for $C_{26}H_{37}ClNaO_6$, 503.2171), with 8 degrees of unsaturation. The ^{1}H NMR spectrum (Table 1) showed characteristic signals for a dimethylvinyl group: δ_H 1.67 (s, H_3-12), 1.62 (s, H_3-13), and 5.09 (t, J= 6.3 Hz, H-10), as well as signals for a terminal double bond at δ_H 5.28 (br s) and 5.17 (br s). The ^{13}C NMR spectrum revealed one ketone carbonyl at δ_C 202.4 (C-2) and two ester carbonyls at

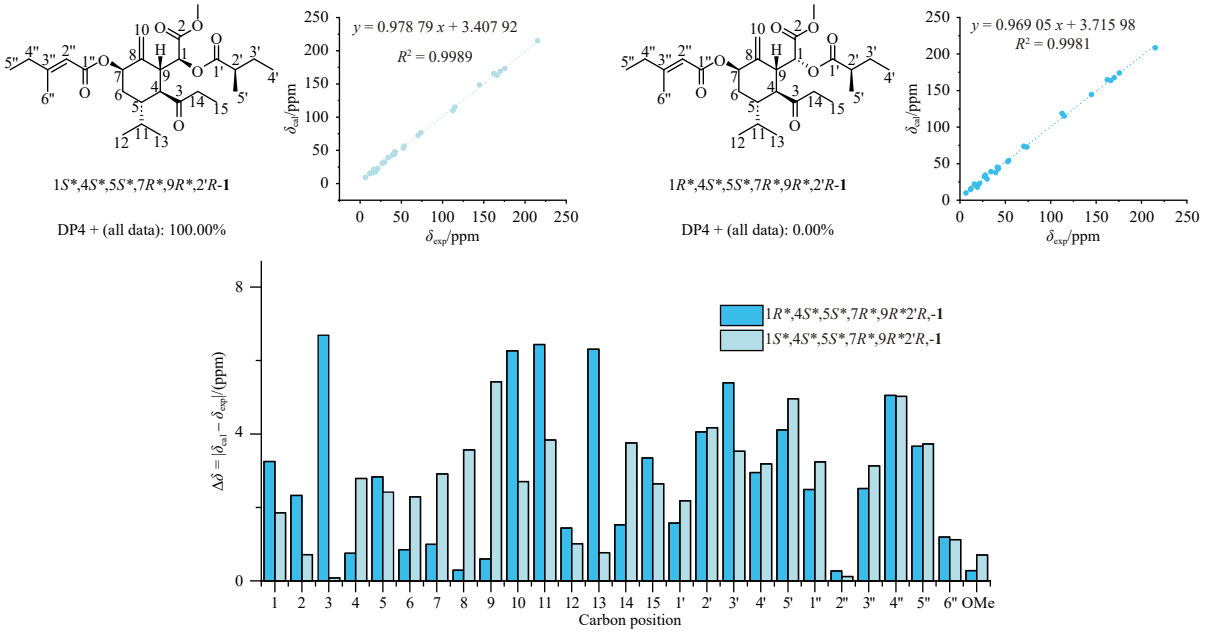

Fig. 4 DP4 + probability analysis, and linear correlation and differential analysis of ^{13}C NMR chemical shift of two possible isomers of **1**.

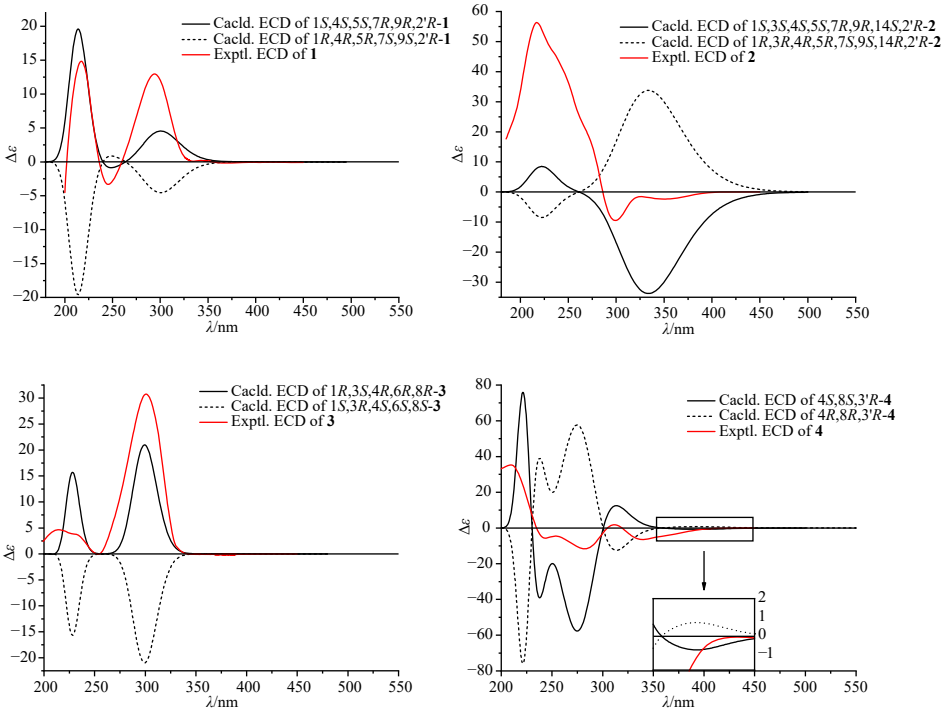

Fig. 5 Experimental ECD curves of compounds **1**–**4** (solid red lines), and M062X/TZVP//B3LYP/6-31G (d) calculated theoretical ECD spectra.

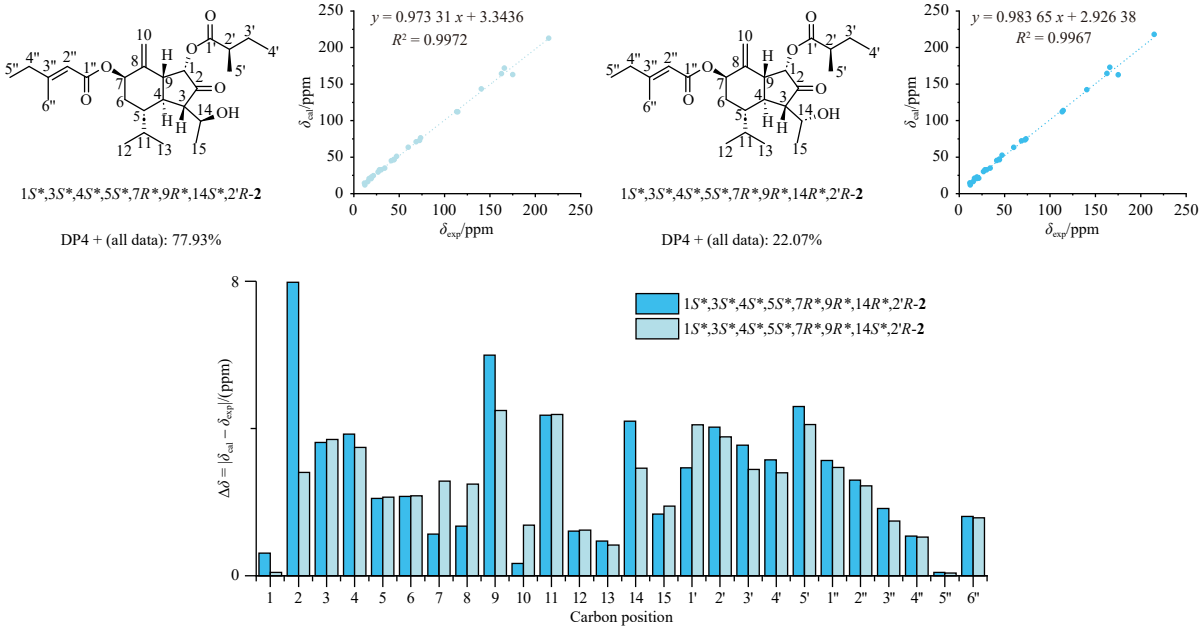

Fig. 6 DP4 + probability analysis, and linear correlation and differential analysis of ^{13}C NMR chemical shift of two possible isomers of **2**.

δ_C 166.6 (C-1′) and 167.7 (C-1″). These data suggested a bisabolane-type sesquiterpene bearing two ester groups and a chlorine substituent, structurally analogous to tussfararin D (**14**) [24] and farfarone A (**15**) [25]. Compared to tussfararin D (**14**), compound **3** contained 14 additional atomic mass units and an extra methyl group at δ_H 1.05 (t, J = 7.53 Hz, H_3-5′), indicating replacement of one angeloyloxy group in **14** with a methyl-senecioyloxy moiety in **3**. The carbon skeleton and remaining substituents were confirmed to be identical to those in **14** and **15** through HSQC, ^{1}H–^{1}H COSY, and HMBC experiments (Fig. 2). Relative configurations at C-1, C-3, C-4, and C-6 were established by NOESY correlations (Fig. 3). The six-membered ring adopted a chair conformation, and the coupling constant $J_{1,6}$ = 12.2 Hz indicated trans-diaxial orientation of H-1 and H-6. H-6 was arbitrarily assigned as β, thus placing H-1 in the α orientation. NOESY correlations of H-1/H-5α, H-5α/H2-14b, H-5β/H-4, and H-4/H_3-15 enabled assignment of relative configurations at C-4 and C-3. NOESY correlations of H-3″ with H-5″ and H-2′ with H2-4′ and H3-5′ indicated Z and E configurations, respectively, for the double bonds in the side chains. Although the relative configuration at C-8 was undetermined in previously reported compounds [24–25], it was resolved in this study *via* quantum chemical calculations. GIAO-based NMR chemical shift calculations were performed for two possible diastereomers—1R^*,3S^*,4R^*,6R^*,8R^*-**3** and 1R^*,3S^*,4R^*,6R^*,8S^*-**3**—at the mPW1PW91/6-311G(d,p) level. The 8R^* isomer exhibited a stronger linear correlation (R^2 = 0.9986) and a DP4 + probability score of 99.96% (Fig. 7). ECD calculations further supported this assignment, as 1R,3S,4R,6R,8R-**3** showed

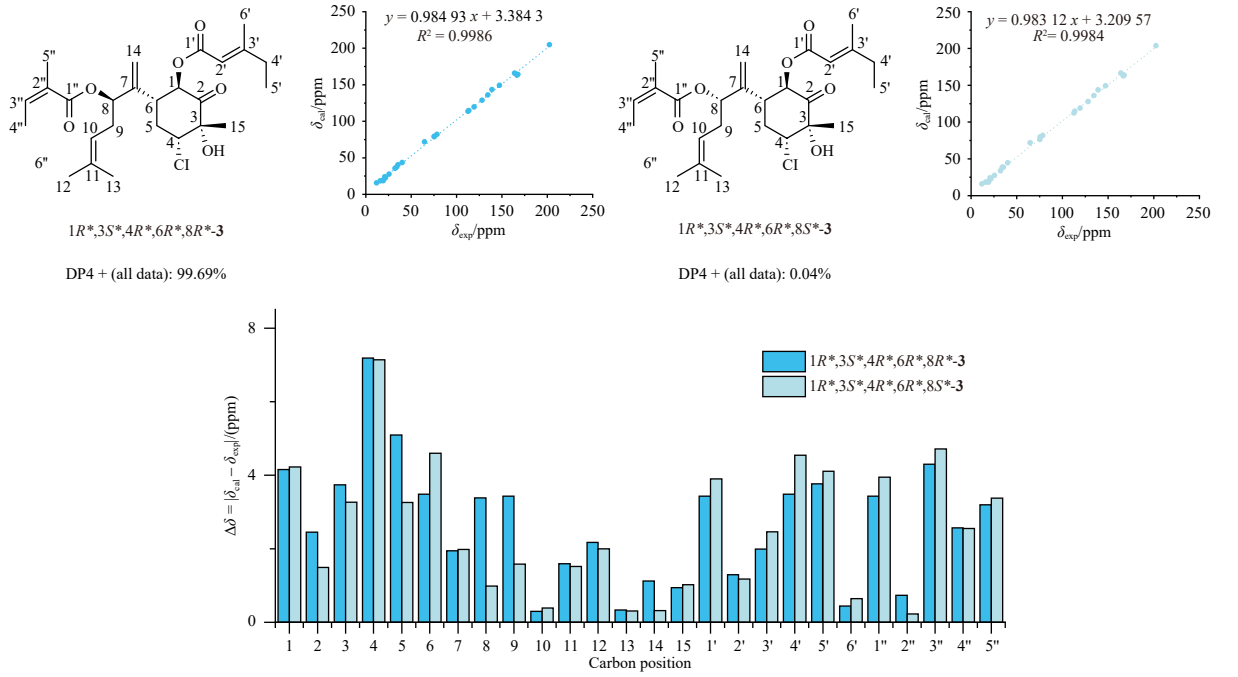

Fig. 7 DP4 + probability analysis, and linear correlation and differential analysis of ^{13}C NMR chemical shift of possible isomers of **3**.

high similarity to the experimental spectrum, displaying first and second positive Cotton effects. Thus, the structure of tussfararin G (**3**) was fully elucidated as shown in Fig. 1.

The molecular formula of tussfararin H (**4**) was determined as $C_{26}H_{38}O_6$ by HR-ESI-MS (*m/z* 469.2568, calculated for $C_{26}H_{38}NaO_6$, 469.2561), indicating 8 degrees of unsaturation. The ^{1}H NMR spectrum (Table 1) revealed eight methyl signals: six olefinic methyls at δ_H 1.98 (br d, *J* = 7.3 Hz), 1.96 (s), 1.95 (s), 1.88 (d, *J* = 1.6 Hz), 1.68 (s), and 1.63 (s) and one terminal methyl at 0.92 (t, *J* = 5.0 Hz). The ^{13}C NMR spectrum showed a conjugated carbonyl at δ_C 183.3, two ester carbonyls at δ_C 171.1 (C-1′) and 168.2 (C-1″), four pairs of double bonds in the range δ_C 118–145, and two oxygen-bearing methines at δ_C 68.6 and 74.3. Comprehensive analysis of these data indicated a dehydrogenated bisabolane-type sesquiterpene, structurally similar to tussfararins E (**22**) and F (**23**) [24]. Compared to tussfararin E (**22**), compound **4** had two additional hydrogen atoms in its molecular formula, suggesting hydrogenation of the methyl-senecioyloxy moiety in **22** to form a 3-methylpentanoyloxy group in **4**, confirmed by an additional methyl doublet at δ_H 1.04 (3H, d, *J* = 5.0 Hz). The planar structure and relative configuration were confirmed by HMBC (Fig. 2) and NOESY (Fig. 3) correlations. NOESY correlations of H-3″/H-5″ indicated a *Z* configuration for the side chain double bond, while H-8/H-5β confirmed an *E* configuration for the 6,7-double bond in the side chain. The absolute configuration at C-3′ of the 3-methylpentanoyloxy group was determined as *R* using the same protocol as for **1**: base hydrolysis, methylation, and chiral GC analysis, comparing the derivative with methylated standards of (*S*)-3-methylpentanoic acid and the racemic mixture. Theoretical NMR chemical shift calculations and ECD computations were conducted for all four possible stereoisomers—4*R*,8*R*,3′*R*-**4**, 4*S*,8*S*,3′*R*-**4**, 4*R*,8*S*,3′*R*-**4**, and 4*S*,8*R*,3′*R*-**4**—to determine relative and absolute configurations (Fig. 8). Among them, 4*S*,8*S*,3′*R*-**4** exhibited the highest linear correlation coefficient (0.9988) and the greatest DP4 + probability score (76.42%). ECD calculations for 4*S*,8*S*,3′*R*-**4** and 4*R*,8*R*,3′*R*-**4** showed that only the former matched the experimental spectrum, displaying first negative, second positive, and third negative Cotton effects (Fig. 4). Therefore, the structure of 4 was assigned accordingly.

By comparing with data reported in the literature, structures of the known sesquitepenoids were determined as farfarone D (**5**) [25], 1α-hydroxy-7β-(4-methylsenecioyloxy)-oplopa-3(14)*Z*, 8(10)-dien-2-one (**6**) [26], 7β-(3'-ethyl-ciscrotonoyloxy)-1α-(2'-methylbutyryloxy)-3,14-dehydro-*Z*-notonipetranone (**7**) [27], (1*S*, 3*S*,4*S*,5*S*,7*R*,9*R*,14*R*)-7β-(3-ethyl-ciscrotonoyloxy)-1α-hydroxynotonipetranone (**8**) [5], 7β-(3-ethyl-ciscrotonoyloxy)-14-hydroxy-1α-(2-methylbutyryloxy)-notonipetranone (**9**) [28], tussfarfarin B (**10**) [29], tussilagofarin (**11**) [30], 14-acetoxy-7β-(3'-ethyl ciscrotonoyloxy)-1α-(2'-methylbutyryloxy)-notonipetranone (**12**) [31], tussilagone (**13**) [27], tussfararin D (**14**) [32], farfarone A (**15**) [25], 1α,5α-diacetoxy-8-angeloyloxy-3β, 4β-epoxybisabola-7(14),10-dien-2-one (**16**) [33], altaicalarins C (**17**) [34], 1α-(3''-ethyl-ciscrotonoyloxy)-8-angeloyloxy-3β,4β-epoxy-bisabola-7(14),10-diene (**18**) [26], 3,4-epoxy-1,8-diangeloyloxybisabola-7(14)-10-dien-2-one (**19**) [35], 8-angeloylxy-3,4-epoxy-bisabola-7(14),10-dien-2-one (**20**) [27], altaicalarin B (**21**) [34], tussfararin E (**22**) [24], and tussfararin F (**23**) [24].

All sesquiterpenoids were evaluated for their potential to enhance insulin-stimulated glucose uptake in C2C12 myotubes. Initially, the cytotoxicity of compounds **1**–**23** was assessed by methyl thiazolyl tetrazolium (MTT) assay to determine maximum safe concentrations. Except for compounds **5**, **6**, **7**, **12**, and **21**, none exhibited significant cytotoxicity toward C2C12 myotubes up to 40 μmol·L^{-1} (Fig. 9A). Subsequently, insulin-stimulated glucose uptake was measured using the 2-NBDG assay at the highest non-toxic concentrations. 5-aminoimidazole-4-carboxamide 1-β-D-ribofuranoside (AICAR) [36] served as the positive control. As shown in Fig. 9B, six out of 23 sesquiterpenoids—compounds **3**, **7**, **10**, **12**, **15**, and **16**—significantly enhanced insulin-stimulated glucose uptake in C2C12 myotubes. Structural analysis and activity data revealed preliminary structure–activity relationships (SAR). For oplopane-type sesquiterpenoids, ester substitution at C-1 enhanced activity (**6** *vs* **7**, **13** *vs* **12**), and etherification at C-14 also increased potency (**9** *vs* **10**). For bisabolane-type sesquiterpenoids, ester groups at C-1 strongly influenced activity (**14** *vs* **15** *vs* **3**), and esterification at C-5 may enhance glucose uptake in 3,4-epoxy-containing scaffolds (**17**–**20** *vs* **16**). Compound 3, the most potent, was selected for further investigation. Notably, it enhanced insulin-stimulated glucose uptake in a dose-dependent manner (Fig. 9C), increasing uptake to approximately 221% at 40 μmol·L^{-1}. To explore the underlying mechanism, key proteins in the insulin signaling pathway were

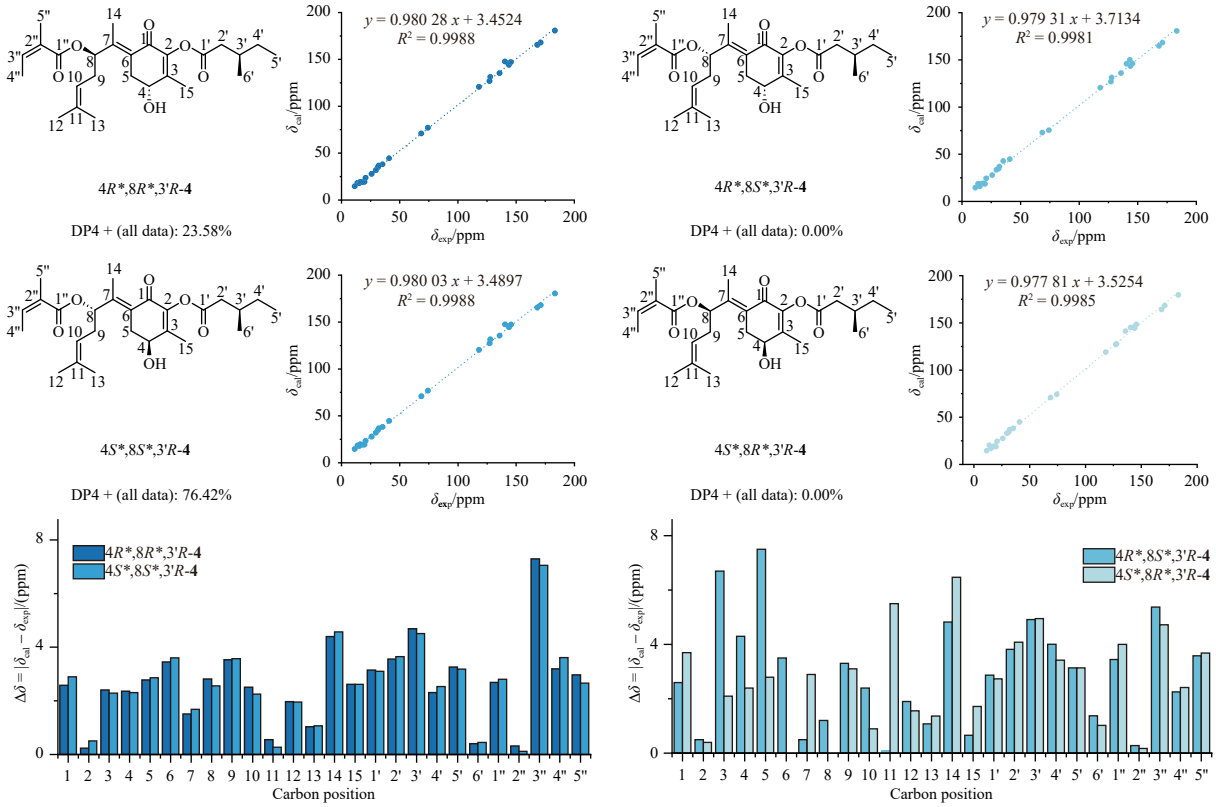

Fig. 8 DP4 + probability analysis, and linear correlation and differential analysis of ^{13}C NMR chemical shift of possible isomers of **4**.

analyzed by Western blot. Insulin binding activates the insulin receptor, leading to phosphorylation of insulin receptor substrate 1 (IRS-1), protein kinase B (Akt), and glycogen synthase kinase 3β (GSK-3β) signaling pathway. Compound **3** further enhanced the phosphorylation of these proteins (Fig. 9D). Taken together, compound **3** improves insulin-stimulated glucose uptake by activating the IRS-1/Akt/GSK-3β signaling pathway in C2C12 myotubes. Based on these findings, *in vivo* biological evaluation of compound **3** is underway. Moreover, hepatocytes represent another valuable model for anti-diabetic drug screening; future studies will assess sesquiterpenoid activities in multiple models to identify additional active compounds.

Inflammation is closely linked to numerous diseases, and many natural products have demonstrated significant anti-inflammatory effects in the lungs [37-38], kidneys [39], and nervous system [40]. Sesquiterpenoids represent an important class of natural anti-inflammatory agents [41]. Therefore, all compounds were tested for their ability to inhibit NO production in LPS-stimulated RAW264.7 macrophages. Cytotoxicity was first evaluated by MTT assay (Fig. 10A). In the NO inhibition assay (Fig. 10B), 21 sesquiterpenoids showed significant inhibitory effects at their maximum safe concentrations. Dexamethasone (Dex) was used as the positive control. Structure–activity relationship analysis indicated that a 1-OH group on the oplopane scaffold enhances anti-inflammatory activity (**13** *vs* **8**; **12** *vs* **8**). For bisabolane-type sesquiterpenoids, the 3,4-epoxy moiety effectively increases activity (**16**, **17**, **20** *vs* **3**, **14**, **15**). Compounds **1**–**4** and **6**, exhibiting strong inhibition, were selected for further study. As shown in Fig. 10C, compounds **1**, **2**, **3**, **4**, and **6** inhibited NO production in a dose-dependent manner. Immunoblotting revealed that compounds **2** and **6** suppressed LPS-induced expression of inducible nitric oxide synthase (iNOS) in a dose-dependent fashion (Fig. 10D). Furthermore, the nuclear factor κB (NF-κB) pathway is a canonical pro-inflammatory signaling cascade. Western blot analysis showed that compounds **2** and **6** inhibited LPS-induced phosphorylation of NF-κB. Collectively, compounds **2** and **6** exert anti-inflammatory effects by suppressing activation of the NF-κB signaling pathway. *In vivo* evaluation of active compounds is ongoing. Growing evidence indicates that low-grade chronic inflammation contributes to insulin resistance [42], while sustained hyperglycemia can trigger inflammatory responses [43]. Notably, compound **3** exhibits both anti-diabetic and anti-inflammatory properties, highlighting its potential as a promising therapeutic agent for diabetes.

3. Conclusion

In summary, four previously undescribed sesquiterpenoids (**1**–**4**), including tussilagofarone (**1**) with a novel 2,3-seco oplopane carbon skeleton, along with 19 known sesquiterpenoids, were isolated from the well-known medicinal plant coltsfoot. Absolute configurations were determined using chemical methods, chiral chromatography, and quantum chemical calculations. All compounds were evaluated for insulin-stimulated glucose uptake in C2C12 myotubes, and compound **3** showed promising activity by activating the IRS-1/Akt/GSK-3β signaling pathway. In the NO inhibition assay using LPS-induced RAW264.7 macrophages, compounds **2** and **6** suppressed LPS-induced iNOS expression and NF-κB phosphorylation in a dose-dependent manner.

4. Experimental

4.1. General experimental procedures

Optical rotations were determined on an Anton Paar MCP 200 automatic polarimeter (Graz, Austria). Ultraviolet (UV) spectra were recorded on a Shimadzu UV-2600 UV-Visible spectrometer in MeOH. ECD spectra were measured on a Chirascan spectrometer (England, United Kingdom). IR spectra were acquired on a Thermo Scientific Fourier Transform NICOLET iS5 Infrared Spectrometer (Waltham, USA) using KBr disks with a DTGS pyro-

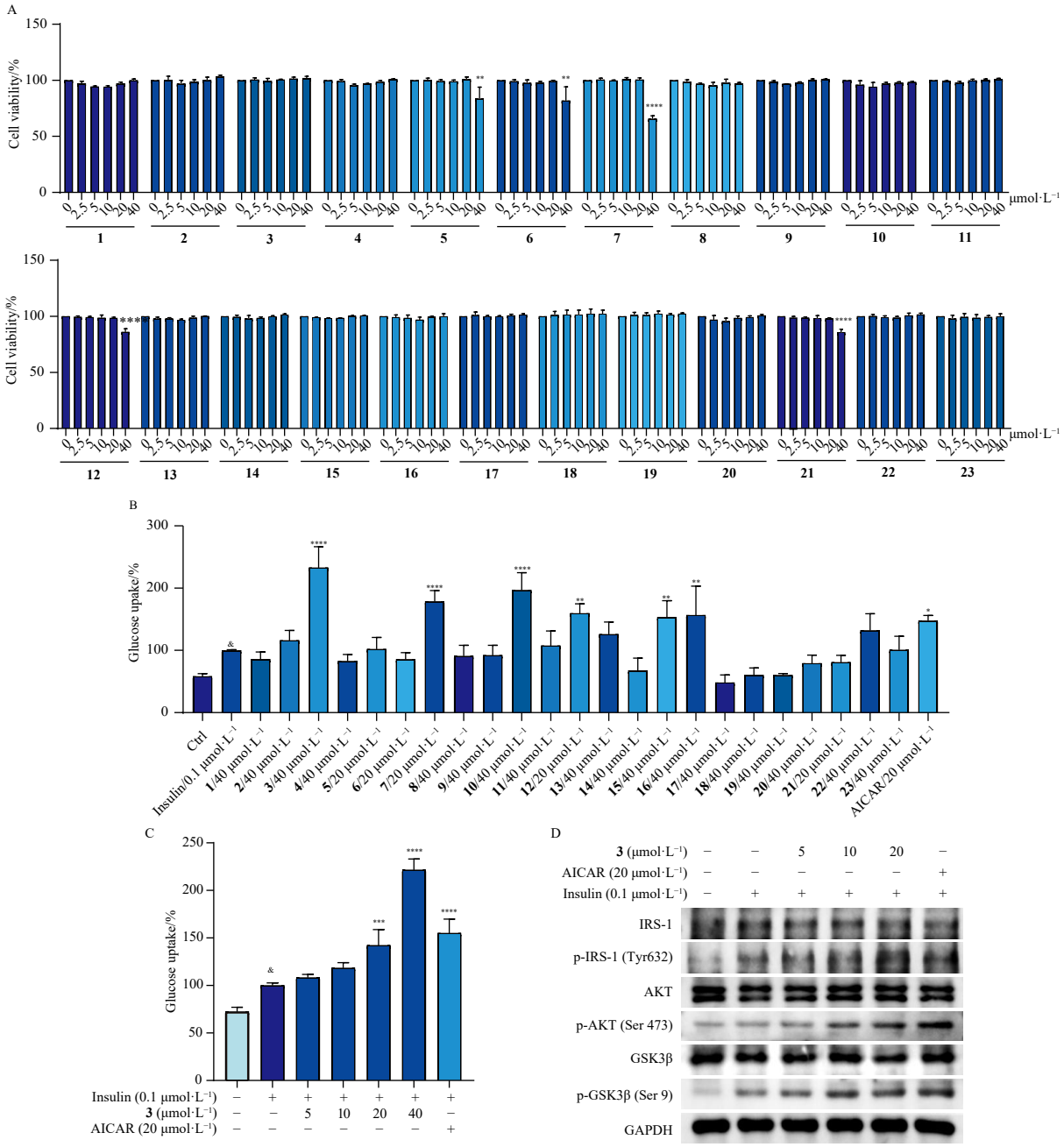

Fig. 9 Compound **3** enhanced insulin-stimulated glucose uptake in C2C12 myotubes. (A) Cytotoxicity of compounds on C2C12 myotubes by MTT assay. (B) Screening of insulin-stimulated glucose uptake on C2C12 myotubes. n=3. (C) Compound **3** increased insulin-stimulated glucose uptake dose-dependently. (D) Compound **3** activated the phosphorylation of proteins associated with the insulin signaling pathway. Data were presented as the means ± SD (n = 3). $^{*}P < 0.05$, $^{**}P < 0.01$, $^{***}P < 0.001$, $^{****}P < 0.0001$.

electric detector (three scans, 4000–400 cm^{-1} with 1.0 cm^{-1} resolution). HR-ESI-MS was measured on an AB SCIEX X500R QTOF mass spectrometry. 1D and 2D NMR data were recorded on a Bruker AVANCE NEO 500 spectrometer (Bremen, Germany) using methanol-d_4 as solvent. Chemical shift values were expressed in δ (ppm) relative to tetramethylsilane (TMS) as the internal standard. Precoated silica gel 60 GF_{254} plates (Branch of Qingdao Haiyang Chemical Co., Ltd., Qingdao, China) were used for thin-layer chromatography (TLC). Silica gel (200–300 mesh and 300–400 mesh, Branch of Qingdao Haiyang Chemical Co., Ltd., Qingdao, China), silica gel for chromatography C18 MB 100-40/75 (Fuji Chemical Industries Co., Ltd., Japan), and D-101 macroporous resin (Shanghai Macklin Biochemical Co., Ltd., Shanghai, China) were employed for column chromatography (CC). A Waters 1500-Series system was used for high-performance liquid chromatography (HPLC) separations. For reversed-phase semipreparative HPLC, a YMC Pack ODS-A C18 (250 mm × 10 mm, 5 μm) column was utilized.

4.2. Plant material

Dried flower buds of *T. farfara* were purchased from Guangzhou Chengji Pharmaceutical Co., Ltd. and authenticated by Professor Jianxia Mo, Institute of Modern Chinese Medicine, Zhejiang University. The quality complies with the standard described in the 'Chinese Pharmacopoeia 2020 Edition'. A voucher specimen (TF2021A) has been deposited in the School of Pharmacy and Food Engineering, Wuyi University.

4.3. Extraction and isolation

A total of 10 kg of dried flower buds was pulverized and extracted with 95% ethanol at room temperature (three successive extractions, each lasting 7 days). The combined ethanol extracts

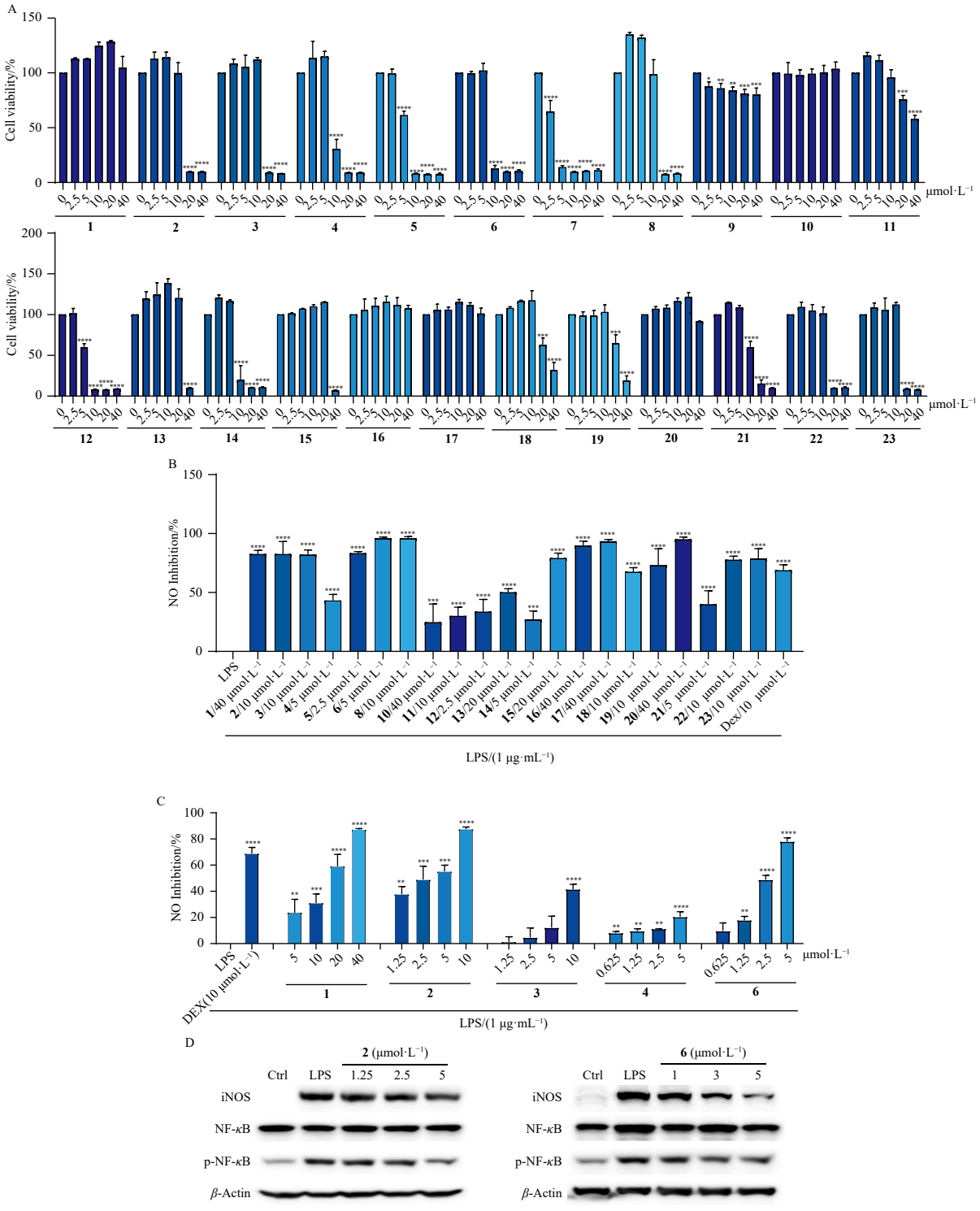

Fig. 10 Compounds inhibited NF-κB activation in LPS-stimulated RAW264.7 cells. (A) Cytotoxicity of compounds in RAW264.7 cells was detected by MTT assay. (B) Inhibitory rate of NO production for compounds. (C) Compounds **1**, **2**, **3**, **4**, and **6** inhibit NO production in a dose-dependent manner. (D) The protein levels of iNOS, NF-κB, and phospho-NF-κB were detected by Western blot analyses. Data were presented as the means ± SD (n = 3). $^{*}P < 0.05$, $^{**}P < 0.01$, $^{***}P < 0.001$, $^{****}P < 0.0001$.

were concentrated under reduced pressure to yield 1.5 kg of crude extract. This residue was suspended in 2.0 L of distilled water and subsequently partitioned three times with petroleum ether, ethyl acetate (EtOAc), and *n*-butanol (*n*-BuOH), respectively. The solvent partitions afforded three fractions: petroleum ether (PE, 234 g), ethyl acetate (EA, 160 g), and *n*-butanol (Bu, 260 g). The PE fraction was subjected to silica gel CC (3000 g, 300–400 mesh) using a gradient elution system (petroleum ether∶ethyl acetate, 1∶0 → 100∶1 → 50∶1 → 30∶1 → 20∶1 → 10∶1, each 3000 mL) to yield three sub-fractions: PEA, PEB, and PEC. The PEC fraction (80 g) was further purified on a D101 macroporous resin column (1000 g) with a gradient elution of 30% to 95% ethanol to give fractions PEC-I–PEC-IV. The PEC-II fraction was subjected to silica gel CC (300–400 mesh) with a gradient elution of petroleum ether∶ethyl acetate (50∶1 → 30∶1 → 20∶1 → 10∶1, each 1000 mL) to yield compounds **16** (5.0 g), **17** (593.0 mg), and **15** (20.0 mg), and the sub-fraction PEC-II-3. The PEC-II-3 fraction was further purified by Sephadex LH-20 CC using dichloromethane: methanol (1∶1) as the mobile phase, resulting in three sub-fractions. These were further separated by semi-preparative HPLC with a CH_3CN–H_2O solvent system at a flow rate of 2 mL·min^{-1}, affording compounds **8** (30.0 mg, t_R = 13.0 min,

$CH_3CN–H_2O$ = 1.8∶0.2), **12** (40.0 mg, t_R = 18.0 min, $CH_3CN–H_2O$ = 1.8∶0.2, *V*/*V*), **14** (10.0 mg, t_R = 19.0 min, $CH_3CN–H_2O$ = 1.8∶0.2, *V*/*V*), and **22** (5.0 mg, t_R = 21.0 min, $CH_3CN–H_2O$ = 1.8∶0.2, *V*/*V*) from the first sub-fraction; compound **20** (4.0 mg, t_R = 16.0 min, $CH_3CN–H_2O$ = 1.5∶0.5, *V*/*V*) from the second; compounds **19** (10.0 mg, t_R = 16.0 min, $CH_3CN–H_2O$ = 1.8∶0.2, *V*/*V*), **18** (30.0 mg, t_R = 20.0 min, $CH_3CN–H_2O$ = 1.8∶0.2, *V*/*V*), and **21** (6.0 mg, t_R = 32.0 min, $CH_3CN–H_2O$ = 1.8∶0.2, *V*/*V*) from the third. Fr. PEC-III was subjected to silica gel CC (300–400 mesh, 400 g) with a gradient elution of petroleum ether-ethyl acetate (50∶1 → 30∶1 → 20∶1 → 10∶1, each 500 mL) to afford seven sub-fractions, which were further purified by semi-preparative HPLC using a $CH_3CN–H_2O$ solvent system at 2 mL·min^{-1}. This separation yielded compound **1** (22.2 mg, t_R = 12.0 min, $CH_3CN–H_2O$ = 1.8∶0.2, *V*/*V*); compounds **2** (20.0 mg, t_R = 9.0 min, $CH_3CN–H_2O$ = 1.5∶0.5, *V*/*V*), **4** (5.0 mg, t_R = 10.0 min, $CH_3CN–H_2O$ = 1.5∶0.5, *V*/*V*), **23** (19.2 mg, t_R = 11.0 min, $CH_3CN–H_2O$ = 1.5∶0.5, *V*/*V*), and **3** (20.0 mg, t_R = 12.0 min, $CH_3CN–H_2O$ = 1.5∶0.5, *V*/*V*); compound **13** (21.0 mg, t_R = 20.0 min, $CH_3CN–H_2O$ = 1.8∶0.2, *V*/*V*); compound **6** (30.0 mg, t_R = 19.0 min, $CH_3CN–H_2O$ = 1.3∶0.7, *V*/*V*); compounds **11** (6.2 mg, t_R = 7.0 min, $CH_3CN–H_2O$ = 1.8∶0.2, *V*/*V*), **10** (10.0 mg, t_R = 12.0 min, $CH_3CN–H_2O$, 1.8∶0.2, *V*/*V*), and **9** (10.2 mg, t_R = 18.0 min, $CH_3CN–H_2O$ = 1.8∶0.2, *V*/*V*); and compounds **5** (10.0 mg, t_R = 12.0 min, $CH_3CN–H_2O$, 1.5∶0.5, *V*/*V*) and **7** (20.0 mg, t_R = 17.0 min, $CH_3CN–H_2O$ = 1.4∶0.6, *V*/*V*).

4.4. Identification of new compounds

*Tussilagofarone (**1**)*: colorless oil; $[\alpha]_D^{27}$ −10.0 (*c* 0.2, MeOH); CD (*c* = 1 mg·mL^{-1}, MeOH) λ_{max} ($\Delta\varepsilon$): 295 (+12.25), 245 (−3.28), 215 (+16.96); UV (MeOH) λ_{max} (log ε): 202 (3.50) nm; IR (KBr) ν_{max}: 3424, 2960, 2932, 1744, 1711, 1648, 1461, 1379, 1221, 1144, 1084 cm^{-1}; ^{1}H and ^{13}C NMR, see Table 1; (+)-HR-ES-IMS *m/z* 501.2825 $[M + Na]^+$ (Calcd. for $C_{27}H_{42}NaO_7$, 501.2823).

*7β-[3′-Ethylcrotonoyloxy]-14-epi-hydroxy-lα-[2′-methylbutyryloxy]-notonipetranone (**2**)*: Colorless oil; $[\alpha]_D^{27}$ −89.9 (*c* 0.2, MeOH); CD (*c* = 1 mg·mL^{-1}, MeOH) λ_{max} ($\Delta\varepsilon$): 298 (−17.60), 211 (+91.41); UV (MeOH) λ_{max} (log ε): 235 (4.17) nm; IR (KBr) ν_{max}: 3446, 2925, 1652, 1456, 1380, 1229, 1145, 1081 cm^{-1}; ^{1}H and ^{13}C NMR, see Table 1; (+)-HR-ESI-MS *m/z* 471.2709 $[M + Na]^+$ (Calcd. for $C_{26}H_{40}NaO_6$, 471.2717).

*Tussfararin G (**3**)*: colorless oil; $[\alpha]_D^{27}$ −84.9 (*c* 0.2, MeOH); CD (*c* = 1 mg·mL^{-1}, MeOH) λ_{max} ($\Delta\varepsilon$): 301 (+30.97), 214 (+4.83); UV (MeOH) λ_{max} (log ε): 209 (3.97) nm; IR (KBr) ν_{max}: 3446, 2929, 1646, 1457, 1382, 1230, 1147, 1085 cm^{-1}; ^{1}H and ^{13}C NMR, see Table 1; (+)-HR-ESI-MS *m/z* 503.2167 $[M + Na]^+$ (Calcd. for $C_{26}H_{37}NaClO_6$, 503.2171).

*Tussfararin H (**4**)*: colorless oil; $[\alpha]_D^{27}$ −14.9 (*c* 0.2, MeOH); CD (*c* = 1 mg·mL^{-1}, MeOH) λ_{max} ($\Delta\varepsilon$): 338 (−0.95), 311 (+0.36), 283 (−1.70), 199 (+4.86); UV (MeOH) λ_{max} (log ε): 205 (3.95) nm; IR (KBr) ν_{max}: 3449, 2922, 1646, 1458, 1378, 1231, 1144, 1041, 973 cm^{-1}; ^{1}H and ^{13}C NMR, see Table 1; (+)-HR-ESI-MS *m/z* 469.2563 $[M + Na]^+$ (Calcd. for $C_{26}H_{38}NaO_6$, 469.2561).

4.5. Hydrolysis, methylation, and chiral GC-MS analysis of ester substituents

Each compound (1.0 mg) was placed in a round-bottomed flask containing 1.0 mL of 50% ethanol, and 0.5 mL of 0.1 mg·mL^{-1} NaOH solution was slowly added. The reaction mixture was refluxed at 95 °C for 12 h, with progress monitored by TLC (petroleum ether∶ethyl acetate, 4∶1, *V*/*V*). Subsequently, the mixture was diluted with saturated sodium chloride solution and extracted with EtOAc. The EtOAc layer was discarded, and the aqueous phase was concentrated. The pH was adjusted to 1–2, followed by extraction with dichloromethane. The dichloromethane layer was evaporated to dryness. Methanol (5 mL) and 0.1 mL of concentrated sulfuric acid were added to the residue, and the mixture was stirred at 80 °C for 12 h. The pH was then adjusted to 7.0 with saturated aqueous $NaHCO_3$. The mixture was extracted with EtOAc, and the organic layer was evaporated to dryness and subjected to chiral GC-MS analysis. Standard compounds—(*S*)-2-methylbutyric acid, (*R*)-2-methylbutyric acid, (*S*)-3-methylpentanoic acid, and (*R*,*S*)-3-methylpentanoic acid—were methylated using the same protocol [44].

Chiral analyses of methyl esters were performed using an Agilent 7890A gas chromatograph equipped with a hydrogen flame ionization detector and an HP-CHIRAL gas chromatographic column (30 m × 320 μm, 0.25 μm). Detector conditions: temperature 260 °C, hydrogen flow rate 35 mL·min^{-1}, air flow rate 350 mL·min^{-1}. Chromatographic conditions: injection volume 1 μL, constant flow rate 1.5 mL·min^{-1}, split ratio 5∶1, temperature program held at 60 °C for 5 min, ramped at 20 °C·min^{-1} to 200 °C, and held for 5 min.

4.6. Quantum chemical calculations

The relative configurations of the side chains in compounds **1**–**4** were determined by quantum chemical calculation of their NMR chemical shifts and comparison with experimental data. Conformational analysis was first performed *via* Monte Carlo searching using molecular mechanics with the MMFF force field in Spartan 18 (Wavefunction Inc., Irvine, CA). The lowest-energy conformers were reoptimized using DFT at the B3LYP/6-31G(d) level in the gas phase with Gaussian 09 [45]. Conformers within 2 kcal·mol^{-1} of the global minimum were included in subsequent steps. GIAO calculations of ^{1}H and ^{13}C NMR chemical shifts were conducted at the rmPW1PW91/6-31 + g (d,p) level in the gas phase [46]. The calculated NMR data for each compound were averaged according to Boltzmann distribution theory based on relative Gibbs free energy (ΔG). Chemical shifts for TMS were calculated using the same protocol and employed as the reference standard. Experimental and calculated data were analyzed using the improved DP4 + probability method for distinguishing isomeric compounds [46], supplemented by linear regression analysis and differential comparison of ^{13}C NMR chemical shifts.

The absolute configurations of compounds **1**–**4** were determined by quantum chemical calculation of their theoretical ECD spectra. Electronic excitation energies and rotatory strengths (velocity) of the first 60 excited states of the DFT-optimized lowest-energy conformers were calculated using TDDFT at the M06-2X/TZVP level in the gas phase. ECD spectra were simulated using overlapping Gaussian functions [47], incorporating velocity-based rotatory strengths from selected excited states (see Supplementary Data). Final ECD spectra were obtained by averaging the simulated spectra of the lowest-energy conformers according to Boltzmann distribution and ΔG.

4.7. Insulin-stimulated glucose uptake in C2C12 myotubes

Mouse C2C12 myoblasts were obtained from American Type Culture Collection (Manassas, VA, USA) and maintained in DMEM with 10% FBS and 1% P/S. When cell confluence reached 100%, C2C12 myoblasts were induced to differentiate in DMEM containing 2% heat-inactivated HS for 5 days. Medium was changed every day to provide adequate nutrition. In cell-based assays, the final DMSO concentration was less than 0.1%.

Cell viability was assessed by MTT assay as previously described. Briefly, C2C12 myoblasts were seeded in 96-well plates at a density of 1 × 10^4 cells per well. After differentiation, cells were treated with DMSO or varying concentrations of test compounds for 24 h. Viability was determined by incubating with MTT (1 mg·mL^{-1}) for 4 h, followed by dissolution of formazan crystals in 100 μL DMSO. Absorbance at 570 nm was measured

using a SpectraMax M5 microplate reader (Molecular Devices, CA, USA).

C2C12 myotubes were incubated with various concentrations of compounds for 24 h, with 20 μmol·L^{-1} AICAR serving as a positive control. Cells were washed with Krebs-Ringer's phosphate (KRP) buffer (20 mmol·L^{-1} HEPES, 137 mmol·L^{-1} NaCl, 4.7 mmol·L^{-1} KCl, 1.2 mmol·L^{-1} $MgSO_4$, 1.2 mmol·L^{-1} KH_2PO_4, 2.5 mmol·L^{-1} $CaCl_2$, and 2 mmol·L^{-1} pyruvate; pH 7.4) and then starved in KRP buffer containing 0.2% bovine serum albumin for 3 h. Subsequently, cells were stimulated with or without 0.1 μmol·L^{-1} insulin for 30 min at 37 °C. Following another wash with KRP buffer, cells were incubated with 100 μmol·L^{-1} 2-NBDG in KRP buffer for 30 min. Fluorescence intensity of 2-NBDG was measured using a microplate reader (Ex/Em: 475/550 nm).

C2C12 myotubes were lysed on ice for 30 min with cold RIPA buffer containing freshly added phosphatase inhibitor cocktails and phenylmethylsulfonyl fluoride (PMSF). Whole-cell lysates were centrifuged at 12 500 r·min^{-1} for 30 min, and supernatants were transferred to new tubes. Protein concentrations were quantified using a BCA protein assay kit (Life Technologies, Grand Island, NY, USA). Equal amounts of protein (30 μg) were separated by 10% SDS-PAGE, transferred to PVDF membranes (Bio-Rad Laboratories, Inc.), blocked with 5% non-fat milk in Tris-buffered saline-Tween 20 (TBST) buffer (100 mmol·L^{-1} NaCl, 10 mmol·L^{-1} Tris-HCl, pH 7.5, 0.1% Tween-20) for 2 h at room temperature, and incubated with specific primary antibodies overnight at 4 °C. After three TBST washes, horseradish peroxidase-conjugated secondary antibody was applied and incubated for 2 h at room temperature. Signals were developed using Super-Signal West Femto Maximum Sensitivity Substrate (Thermo, Rockford, IL, USA). Specific protein bands were visualized using the ChemiDoc MP Imaging System and quantified with Image Lab 5.1 (Bio-Rad, Hercules, CA, USA).

4.8. LPS-stimulated NO production in RAW264.7 cells

The anti-inflammatory assay and mechanistic studies were conducted following the same protocol as in previous reports [48]. Briefly, RAW264.7 macrophages were cultured, and MTT assays were performed to assess cell viability for all compounds. NO production was quantified using Griess reagent. Protein expression was evaluated by Western blot analysis.

4.9. Statistical analysis

All data are presented as mean ± SD from at least three independent experiments and analyzed using GraphPad Prism 6 (GraphPad Software, San Diego, CA, USA). One-way ANOVA was used for statistical comparisons, with $^{*}P < 0.05$ considered statistically significant.

Funding

This work was supported by the National Natural Science Foundation of China (No. 22077111), the Department of Education of Guangdong Province (No. 2022ZDJS025), the Hong Kong/Macao Joint Research and Development Fund Project of Wuyi University (No. 2022WGALH15), and Zhejiang Medical and Health Science and Technology Plan Project of China (No. 2022KY231).

Supporting information

Supplementary data associated with this article can be requested by sending E-mail to the corresponding authors.

Declaration of competing interest

These authors have no conflict of interest to declare.

References

1 Editorial Committee of Flora of China. *Flora of China*. Beijing: Science Press. 1999;77(1):93.
2 Chen SJ, Dong L, Quan HF, et al. A review of the ethnobotanical value, phytochemistry, pharmacology, toxicity and quality control of *Tussilago farfara* L. (coltsfoot). *J Ethnopharmacol*. 2021;267:113478. https://doi.org/10.1016/j.jep.2020.113478.
3 Liu C, Wu HW, Wang LX, et al. Farfarae Flos: a review of botany, traditional uses, phytochemistry, pharmacology, and toxicology. *J Ethnopharmacol*. 2020;260:113038. https://doi.org/10.1016/j.jep.2020.113038.
4 Li YP, Yang K, Meng H, et al. Polyhydroxylated eudesmane sesquiterpenoids and sesquiterpenoid glucoside from the flower buds of *Tussilago farfara*. *Chin J Nat Med*. 2022;20(4):301-308. https://doi.org/10.1016/S1875-5364(21)60120-6.
5 Song XQ, Yu JH, Sun J, et al. Bioactive sesquiterpenoids from the flower buds of *Tussilago farfara*. *Bioorg Chem*. 2021;107:104632. https://doi.org/10.1016/j.bioorg.2021.104632.
6 Song XQ, Sun J, Yu JH, et al. Prenylated indole alkaloids and lignans from the flower buds of *Tussilago farfara*. *Fitoterapia*. 2020;146:104729. https://doi.org/10.1016/j.fitote.2020.104729.
7 Cheng XY, Liao M, Diao XP, et al. Screening and identification of metabolites of two kinds of main active ingredients and hepatotoxic pyrrolizidine alkaloids in rat after lavage Farfarae Flos extract by UHPLC-Q-TOF-MS mass spectrometry. *Biomed Chromatogr*. 2018;32(2):4047. https://doi.org/10.1002/bmc.4047.
8 Sun MJ, Li Y, Su ST, et al. Tussilagone ameliorates high-fat diet-induced hepatic steatosis by enhancing energy metabolism and antioxidant activity. *Phytother Res*. 2024;38(5):2099-2113. https://doi.org/10.1002/ptr.7818.
9 Feng XL, Liu ZJ, Su YG, et al. Tussilagone inhibits osteoclastogenesis by modulating mitochondrial function and ROS production involved in Nrf2 activation. *Biochem Pharmacol*. 2023;218:115895. https://doi.org/10.1016/j.bcp.2023.115895.
10 Song K, Nho CW, Ha IJ, et al. Cellular target proteome in breast cancer cells of an oplopane sesquiterpenoid isolated from *Tussilago farfara*. *J Nat Prod*. 2020;83:2559-2566. https://doi.org/10.1021/acs.jnatprod.0c00043.
11 Zhou J, Yang RP, Song W, et al. Antiplatelet activity of tussilagone *via* inhibition of the GPVI downstream signaling pathway in platelets. *Front Med (Lausanne)*. 2020;7:380. https://doi.org/10.3389/fmed.2020.00380.
12 Lim HJ, Dong GZ, Lee HJ, et al. *In vitro* neuroprotective activity of sesquiterpenoids from the flower buds of *Tussilago farfara*. *J Enzyme Inhib Med Chem*. 2015;30:852-856. https://doi.org/10.3109/14756366.2014.965701.
13 Feng ZL, Fang ZJ, Chen C, et al. Anti-hyperglycemic effects of refined fractions from *Cyclocarya paliurus* leaves on streptozotocin-induced diabetic mice. *Molecules*. 2021;26:22. https://doi.org/10.3390/molecules26226886.
14 Zhang LS, Shen SN, Gao YL, et al. Tautomerism and bioactivities of curcumenol, a common sesquiterpenoid widely existing in edible plants. *Food Funct*. 2019;10:1288-1294. https://doi.org/10.1039/c8fo02549e.
15 Fang ZJ, Shen SN, Wang JM, et al. Triterpenoids from *Cyclocarya paliurus* that enhance glucose uptake in 3T3-L1 adipocytes. *Molecules*. 2019;24:187. https://doi.org/10.3390/molecules24010187.
16 Lee SH, Park SY, Choi CS. Insulin resistance: from mechanisms to therapeutic strategies. *Diabetes Metab J*. 2022;46:15-37. https://doi.org/10.4093/dmj.2021.0280.
17 Merz K, Thurmond D. Role of skeletal muscle in insulin resistance and glucose uptake. *Compr Physiol*. 2020;10:785-809. https://doi.org/10.1002/cphy.c190029.
18 DeFronzo RA, Tripathy D. Skeletal muscle insulin resistance is the primary defect in type 2 diabetes. *Diabetes Care*. 2009;32(Suppl.2):S157-S163. https://doi.org/10.3390/nu14030647.
19 Lucia M, Michael R. Insulin resistance and insulin sensitizing agents. *Metabolism*. 2021;125:154892. https://doi.org/10.1016/j.metabol.2021.154892.
20 Li J, Xue YM, Zhu B, et al. Rosiglitazone elicits an adiponectin-mediated insulin-sensitizing action at the adipose tissue-liver axis in Otsuka Long-Evans Tokushima fatty rats. *J Diabetes Res*. 2018;2018:4627842. https://doi.org/10.1155/2018/4627842.
21 Feng J, Wang XH, Ye XC, et al. Mitochondria as an important target of metformin: the mechanism of action, toxic and side effects, and new therapeutic applications. *Pharmacol Res*. 2022;177:106114. https://doi.org/10.1016/j.phrs.2022.106114.
22 Masao K, Noriko S. Studies on the constituents of *Tussilago farfara* L. II. Structures of new sesquiterpenoids isolated from the flower buds. *Chem Pharm Bull*. 1992;40:2753-2755. https://doi.org/10.1248/cpb.40.2753.
23 Bohlmann F, Zdero C, Gupta RK. Notonipetrone-like sesquiterpenes from *Senecio Kleinia*. *Phytochemistry*. 1981;20:2024-2026. https://doi.org/10.1016/0031-9422(81)84059-9.
24 Qin ZB, Zhang J, Wu XD, et al. Sesquiterpenoids from *Tussilago farfara* and their inhibitory effects on nitric oxide production. *Planta Med*. 2014;80:703-709. https://doi.org/10.1055/s-0034-1368567.
25 Xu J, Sun XC, Kang J, et al. Chemical and biological profiles of *Tussilago farfara*: Structures, nitric oxide inhibitory activities, and interactions with iNOS protein. *J Funct Foods*. 2017;32:37-45. https://doi.org/10.1016/j.jff.2017.02.013.
26 Wei L, Xin H, Yang XW. New sesquiterpenoids from the dried flower buds of *Tussilago farfara* and their inhibition on NO production in LPS-induced RAW264.7 cells. *Fitoterapia*. 2012;83:318-322. https://doi.org/10.1016/j.fitote.2011.11.011.
27 Park HR, Yoo MY, Seo JH, et al. Sesquiterpenoids isolated from the flower buds of *Tussilago farfara* L. inhibit diacylglycerol acyltransferase. *J Agric*

Food Chem. 2008;56:10493-10497. https://doi.org/10.1021/jf801978r.
28 Wang Q, Chen TH, Bastow KF, et al. Altaicalarins A–D, cytotoxic bisaboline sesquiterpenes from *Ligularia altaica*. *J Nat Prod*. 2010;73:139-142. https://doi.org/10.1021/np900489h.
29 Liu LL, Yang JL, Shi YP. Sesquiterpenoids and other constituents from the flower buds of *Tussilago farfara*. *J Asian Nat Prod Res*. 2011;13:920-929. https://doi.org/10.1080/10286020.2011.600251.
30 Jang H, Lee JW, Lee C, et al. Sesquiterpenoids from *Tussilago farfara* inhibit LPS-induced nitric oxide production in macrophage RAW 264.7 cells. *Arch Pharm Res*. 2016;39:127-132. https://doi.org/10.1007/s12272-015-0667-7.
31 Wang DJ, Fang L, Wang X, et al. Preparative separation and purification of sesquiterpenoids from *Tussilago farfara* L. by high-speed counter-current chromatography. *Quim Nova*. 2011;34:804-807. https://doi.org/10.1590/S0100-40422011000500014.
32 Wang S, Jin DQ, Xie C, et al. Isolation, characterization, and neuroprotective activities of sesquiterpenes from *Petasites japonicus*. *Food Chem*. 2013;141:2075-2082. https://doi.org/10.1016/j.foodchem.2013.04.116.
33 Yaoita Y, Suzuki N, Kikuchi M. Structures of new sesquiterpenoids from Farfarae flos. *Chem Pharm Bull*. 2001;49:645-648. https://doi.org/10.1248/cpb.49.645.
34 Shu HZ, Peng C, Bu L, et al. Bisabolane-type sesquiterpenoids: structural diversity and biological activity. *Phytochemistry*. 2021;192:112927. https://doi.org/10.1016/j.phytochem.2021.112927.
35 Kang J, Ji F, Yang B, et al. Studies on chemical constituents of the flower buds of *Tussilago farfara*. *J Pharm Res*. 2016;35:373-375. https://doi.org/10.13506/j.cnki.jpr.2016.07.001.
36 Xuan LL, Yang S, Ren LL, et al. Akebia saponin D attenuates allergic airway inflammation through AMPK activation. *J Nat Med*. 2024;78(2):393-402. https://doi.org/10.1007/s11418-023-01762-2.
37 Zhang J, Zhang M, Huo XK, et al. Macrophage inactivation by small molecule wedelolactone *via* targeting sEH for the treatment of LPS-induced acute lung injury. *ACS Cent Sci*. 2023;9(3):440-456. https://doi.org/10.1021/acscentsci.2c01424.
38 Zhang J, Zhang M, Zhu QM, et al. Allosteric regulation of Keap1 by 8*β*-hydroxy-*α*-cyclocostunolide for the treatment of acute lung injury. *Acta Pharm Sin B*. 2024;14:4174-4178. https://doi.org/10.1016/j.apsb.2024.06.025.
39 Zhang J, Luan ZL, Huo XK, et al. Direct targeting of sEH with alisol B alleviated the apoptosis, inflammation, and oxidative stress in cisplatin-induced acute kidney injury. *Int J Biol Sci*. 2023;19:294-310. https://doi.org/10.7150/ijbs.78097.
40 Sun CP, Zhou JJ, Yu ZL, et al. Kurarinone alleviated Parkinson's disease *via* stabilization of epoxyeicosatrienoic acids in animal model. *Proc Natl Acad Sci USA*. 2022;119(9):e2118818119. https://doi.org/10.1073/pnas.2118818119.
41 Zhang J, Yan JK, Dong HJ, et al. Dimeric sesquiterpenoids with anti-inflammatory activities from *Inula britannica*. *Chin J Nat Med*. 2024;22:1-13. https://doi.org/10.1016/S1875-5364(24)60692-8.
42 Garg SS, Kushwaha K, Dubey R, et al. Association between obesity, inflammation and insulin resistance: Insights into signaling pathways and therapeutic interventions. *Diabetes Res Clin Pract*. 2023;200:110691. https://doi.org/10.1016/j.diabres.2023.110691.
43 Berbudi A, Rahmadika NI, Tjahjadi AI, et al. Type 2 diabetes and its impact on the immune system. *Curr Diabetes Rev*. 2020;16:442-449. https://doi.org/10.2174/1573399815666191024085838.
44 Oppolzer W, Dudfield P, Stevenson T, et al. Camphorsulfonamide-shielded, asymmetric 1,4-additions and enolate alkylations; synthesis of a southern corn rootworm pheromone. *Helv Chim Acta*. 1985;68:212-215. https://doi.org/10.1002/hlca.19850680126.
45 Frisch MJ, Trucks GW, Schlegel HB, et al. Gaussian 09, Revision A01. Gaussian, Inc. , Wallingford CT, 2009.
46 Grimblat N, Zanardi MM, Sarotti AM. Beyond DP4: An improved probability for the stereochemical assignment of isomeric compounds using quantum chemical calculations of NMR shifts. *J Org Chem*. 2015;80:12526-12534. https://doi.org/10.1021/acs.joc.5b02396.
47 Stephen PJ, Harada NE. ECD cotton effect approximated by the Gaussian curve and other methods. *Chirality*. 2010;22:229-233. https://doi.org/10.1002/chir.20733.
48 Xu F, Zhang LS, Zhou CX, et al. Alkyl-benzofuran dimers from *Eupatorium chinense* with insulin-sensitizing and anti-inflammatory activities. *Bioorg Chem*. 2021;113:105030. https://doi.org/10.1016/j.bioorg.2021.105030.